

Significance of Absorption Coefficients When Determining In Situ Core Saturations by Linear X-ray Scans

By D. R. Maloney, D. C. Wegener, and D. R. Zornes, Phillips Petroleum Company

Abstract

Linear x-ray scanners are increasingly used to measure fluid saturations in cores during laboratory tests. Reasons include the expanding need to model and measure complex reservoir-condition fluid-flow behavior in the laboratory, availability of ready-made scanners from commercial suppliers, and regulatory and safety issues that limit the applicability of other types of radiation emitting sources.

Lambert's equation is recognized as a basis for understanding x-ray absorption phenomena. This equation relates the intensity of an x-ray beam that emerges from an absorber to the incident beam intensity, absorption coefficients and thickness of absorbers that the beam passes through. Although this relationship is well understood, many x-ray "practitioners" resort to heuristic approaches that correlate emergent beam intensity directly to fluid saturation. Heuristic approaches suffice for relatively simple tests, but are inappropriate when fluid densities and compositions change during a test. Under such circumstances, advantages are gained using a form of Lambert's equation directly with consideration for changes in absorption coefficients.

This paper provides a bridge between x-ray theory and practical applications. Knowledge gained can significantly improve experimental designs and x-ray data analyses such that more accurate saturation measurements can be obtained during difficult reservoir condition tests. Differences among absorption coefficients described in the literature for monochromatic x-rays and those measured in the lab from a polychromatic beam are described. An understanding of these differences provides one with the ability to predict how intensities of polychromatic x-rays will change during a test depending upon compositions, densities, and thickness of absorbers. Simple equations are presented for calculating two- and three-phase saturations from x-ray data.

Background

X-rays have been used to measure fluid saturations in cores for over 50 years. Early investigators¹⁻⁵ proved the capability of x-ray saturation measurements, in spite of complexities imposed by the limited hardware and analytical tools of the era. Hardware and software have significantly improved in recent years, but misconceptions still exist concerning what can and can't be done with x-rays. A review of the literature gives an impression that the polychromatic nature of x-rays is a disadvantage compared to what can be achieved using a monochromatic radiation source. Because of this impression, many labs do not directly apply Lambert's equation but instead resort to heuristic approaches for calibrating and using x-ray data for saturation measurements. Heuristic approaches solve for saturations assuming a simple linear relationship between the

natural logarithm of emergent intensity and fluid saturation. This paper shows that direct application of a form of Lambert's equation and the polychromatic nature of the x-ray beam can be used to great advantage; especially when one understands and uses x-ray absorption coefficients properly.

Figure 1 is a simple schematic of the linear x-ray scan arrangement that we use. The system is described in detail elsewhere⁶. Primary components are the x-ray tube, tube collimator, beam filters, detector collimator, and detector. The low energy germanium detector (Canberra Model GL2020R), multi-channel analyzer (MCA), and associated hardware and software provide measures of photon intensities and potentials of the emergent x-ray spectra. The tube and detector move along 3 axes (vertical, horizontal, and inward or outward) with respect to a stationary sample. For measurements described in this paper, tube-to-sample and detector-to-sample distances were 55 cm. To take full advantage of both intensity and energy measurements, scans consist of move-stop-measure sequences at positions along the length of a sample.

Basic X-ray Phenomena

Lambert's equation⁷ is recognized as a basis for understanding x-ray absorption phenomena. It relates the intensity (E) of a collinear monochromatic x-ray beam that emerges from an absorber of known thickness (t , cm) and linear absorption coefficient (μ , cm^{-1}) to the incident beam intensity (E_0):

$$E = E_0 \exp[-(\mu t)] \quad (1)$$

Intensities are commonly expressed in units of photon counts/live-time second. From idealized measurements with a collinear, monochromatic x-ray beam, one can calculate the thickness of an absorber using equation 1 if incident and emergent intensities and the linear absorption coefficient of the absorber are known:

$$[\text{Ln}(E_0/E)]/\mu = [\text{Ln}(E_0) - \text{Ln}(E)]/\mu = t \quad (2)$$

When several absorbers are placed in the beam path, equation 1 is rewritten as:

$$E = E_0 \exp[-(\mu_A t_A + \mu_B t_B + \mu_C t_C + \dots)] \quad (3)$$

where A, B, C and so forth are different absorbers within the beam path.

Absorption coefficients vary as a function of potential or wavelength. Abrupt changes in absorption occur for each element at particular potentials or wavelengths (absorption edges). A related absorption coefficient, the mass absorption coefficient (μ_p , cm^2/gram) is more readily described in the literature. The mass absorption coefficient is a property of each substance independent of state of physical aggregation.⁷ Graphs and tables in the literature commonly list mass absorption coefficients at various excitation potentials or wavelengths. The linear absorption coefficient can be calculated from the mass absorption coefficient at a particular potential or wavelength if the density (g/cm^3) of the substance at the measurement condition (pressure and temperature) is known:

$$\mu = \mu_p * \rho \quad (4)$$

The mass absorption coefficient of a compound, solution, or mixture of elements can be calculated⁷ if weight fractions (W_i), densities, and absorption coefficients of the constituents are known:

$$(\mu/\rho)_{ABC} = W_A(\mu/\rho)_A + W_B(\mu/\rho)_B + W_C(\mu/\rho)_C \quad (5)$$

Corollary to Lambert's Equation

Lambert's equation is difficult to apply in strict accordance to theory because of difficulties in measuring incident beam intensities. If the incident intensity remains constant (or can be corrected for minor changes in flux), and spacing between the tube, sample, and detector remain constant, a corollary to Lambert's equation is:

$$I = I_o \exp[-(\mu_A t_A + \mu_B t_B + \mu_C t_C + \dots)] \quad (6)$$

This is similar to equation 3 with the following exceptions. Both I_o and I are emergent beam intensities. I_o is the emergent intensity at a reference condition, while I is the emergent intensity after a change in the absorption characteristics or change in thickness of absorbers within the beam path. The thickness variable t now represents the change in thickness of an absorber compared to its thickness when I_o was measured. I_o already accounts for photon absorption by the coreholder, insulating materials, rock matrix, and other materials within the beam path that are expected to retain consistent absorption properties throughout the test.

Single-Phase, Two-Phase, and Three-Phase Calculations

This section describes approaches for calculating multiphase core saturations using equation 6. Consider a dry core within a coreholder under net confining pressure conditions. Assume that the test is such that all changes in emergent x-ray intensity result only from changes in the fluid contents within the rock. Here, I_o is the emergent intensity after the x-ray beam has penetrated the coreholder, confining fluid, core sleeve, dry core, and other materials that are considered "fixed" during the test. After preliminary scans of the rock within the coreholder have identified x-ray tube voltage and current settings that will be used during the test, the intensity measured for the dry core at a particular scan position may be considered as I_o for that scan position. Variables are labeled with subscripts to make it easier to associate measurements with energy ranges (subscript 1,1 stands for energy range 1, fluid 1). The average thickness (D , cm) of the rock that the x-ray beam passes through can be calculated. This average thickness may be less than the diameter of the core because of surface curvature. After changing the saturation condition at a position within the rock, the emergent intensity (I_1) changes according to equation 6 using appropriate thickness and linear absorption values. For instance, if the rock is first completely saturated with fluid 1, solving for t_1 for a particular scan position consists of the following steps:

$$I_1 = I_{o1} \exp[-(\mu_{1,1} t_1)] \quad (7)$$

$$I_1/I_{o1} = \exp[-(\mu_{1,1} t_1)]$$

$$\ln(I_1/I_{o1}) = -\mu_{1,1} t_1$$

$$t_1 = [\ln(I_{o1}/I_1)] / \mu_{1,1} \quad (8)$$

As the rock is now completely saturated with fluid 1, (t_1) is also equal to the total equivalent thickness of fluid within the pore space (T , cm). The porosity fraction of the rock for this particular scan position is:

$$\text{Porosity} = t_1 / D \quad (9)$$

And fluid 1 saturation fraction is $S_1 = t_1 / T = 1.000$

If fluid 2 is now injected into the core, we can solve for the thickness of fluids 1 and 2. If we assume that the porosity of the rock hasn't changed, the total fluid filled thickness still equals (T). Solving for t_1 and t_2 proceeds as:

$$I_1 = I_{o1} \exp[-(\mu_{1,1}t_1 + \mu_{1,2}t_2)]$$

$$\text{Ln}(I_{o1}/I_1) = \mu_{1,1}t_1 + \mu_{1,2}t_2 \quad (10)$$

$$t_2 = T - t_1 \quad (11)$$

$$\text{Ln}(I_{o1}/I_1) = \mu_{1,1}t_1 + \mu_{1,2}(T - t_1)$$

$$[\text{Ln}(I_{o1}/I_1) - \mu_{1,2}(T)] = (\mu_{1,1} - \mu_{1,2})t_1$$

$$t_1 = [\text{Ln}(I_{o1}/I_1) - \mu_{1,2}(T)] / (\mu_{1,1} - \mu_{1,2}) \quad (12)$$

Once t_1 is known, t_2 is calculated from equation 11. Fluid saturation fractions are:

$$S_1 = t_1 / T$$

$$S_2 = t_2 / T$$

and

$$S_1 + S_2 = 1.000$$

The thickness of each fluid can also be calculated without assuming that the porosity is constant. However, an additional equation is needed. Intensity data measured over a second energy range provides another equation. Assuming I_{o2} has been measured, a second equation is:

$$\text{Ln}(I_{o2}/I_2) = \mu_{2,1}t_1 + \mu_{2,2}t_2 \quad (13)$$

Equations 10 and 13 provide a set of linear equations with two unknowns. Applying Cramer's Rule⁸ yields:

$$t_1 = [\mu_{2,2} * \text{Ln}(I_{o1}/I_1) - \mu_{1,2} * \text{Ln}(I_{o2}/I_2)] / [(\mu_{1,1} * \mu_{2,2}) - (\mu_{1,2} * \mu_{2,1})] \quad (14)$$

$$t_2 = [\mu_{1,1} * \text{Ln}(I_{o2}/I_2) - \mu_{2,1} * \text{Ln}(I_{o1}/I_1)] / [(\mu_{1,1} * \mu_{2,2}) - (\mu_{1,2} * \mu_{2,1})] \quad (15)$$

Now, the total fluid-filled thickness within the rock is $t_1 + t_2$. Fluid saturations are:

$$S_1 = t_1 / (t_1 + t_2)$$

$$S_2 = t_2 / (t_1 + t_2)$$

If a third fluid phase (t_3) is introduced into the rock pore space, a similar treatment is applied. With intensity data from two energy ranges, we have:

$$\text{Ln}(I_{o1}/I_1) = \mu_{1,1}t_1 + \mu_{1,2}t_2 + \mu_{1,3}t_3 \quad (16)$$

$$\text{Ln}(I_{o2}/I_2) = \mu_{2,1}t_1 + \mu_{2,2}t_2 + \mu_{2,3}t_3 \quad (17)$$

A third equation is needed. If the rock porosity remains constant, we can assume that the total fluid thickness penetrated by the x-ray beam is a known value (T). The third equation is:

$$t_1 + t_2 + t_3 = T \quad (18)$$

If the linear absorption coefficient of the third phase is so small that the reduction in x-ray intensity by the third fluid phase is insignificant, additional simplifications are:

$$\mu_{1,3}t_3 = 0 \text{ and } \mu_{2,3}t_3 = 0 \quad (19)$$

If neither of the assumptions of equations 18 or 19 are true, a third equation is still needed. An approach used by Laird and Putnam⁵ was to dope two of the fluid phases so that their linear absorption coefficients were approximately equal at one of the two energy ranges but significantly different with the second energy range. This provides a third equation as:

$$\mu_{1,1} = \mu_{1,2} \quad (20)$$

If the simplifying assumptions of equations 18-20 do not apply, then a third equation can be developed by measuring intensities at a third energy range, yielding:

$$\ln(I_{03}/I_3) = \mu_{3,1}t_1 + \mu_{3,2}t_2 + \mu_{3,3}t_3 \quad (21)$$

Cramer's Rule can be used to solve the three linear equations for thickness t_1 , t_2 , and t_3 .

When the core plug is scanned at various positions along its length, saturation calculations at each position are treated separately to account for porosity variation. However, as long as a fluid retains consistent properties throughout a core plug, its linear absorption coefficient is the same at all scan positions. Fluid thickness calculated from a scan at one energy should agree with the thickness calculated from a scan at another energy. Adjustments for changes in linear absorption coefficients because of fluid density changes are straightforward.

Dealing with the Polychromatic Nature of the Spectra

While equation 5 can be used to calculate absorption coefficients for mixtures such as typical test fluids, a method is needed to calculate absorption coefficients for fluids or materials over the range of potentials exhibited by the polychromatic emergent x-ray spectra. XCOM by Berger and Hubble⁸ greatly simplifies this task. The computer program runs efficiently on a PC and accounts for various types of absorption phenomena. XCOM calculates mass absorption coefficients for elements, mixtures, or compounds at specific energies of interest. As an example, XCOM was used to calculate mass absorption coefficients (assuming no coherent scatter) at potentials from 29 keV to 95 keV for water, decane, and brines consisting of water doped with different cesium chloride (CsCl) and potassium bromide (KBr) weight fractions. Results correspond to each of the 1150 MCA channels that our germanium detector uses over this range of potentials. Linear absorption coefficients were then calculated for ambient conditions using equation 4 and appropriate fluid densities. Figure 2 shows these results. Note that absorption characteristics of cesium chloride brines show a discontinuity at slightly less than 36 keV. This is because of the cesium K-absorption edge. Linear absorption coefficients for the fluids at other temperatures and pressures can be calculated if the densities of the fluids are known at the temperatures and pressures of interest.

The following example shows how these fluids affect intensities of x-rays that emerge from a coreholder containing a rock plug. Dry-scan data for this example are

from x-ray scans performed on a dry (air-filled) chalk core plug from a North Sea reservoir. The core was within a carbon fiber composite coreholder with net confining pressure of 70 bars at 20 °C. X-ray scans were performed with tube voltage and current set at 52 kV, 25 mA and again with 95 kV, 5 mA. For the 95 kV measurement, the incident beam was conditioned at the x-ray tube through a filter (cuvette filled with a cesium chloride and water solution) to reduce emergent intensities to levels that could be accurately measured by the detector. Subsequent x-ray measurements after saturating the plug with brine defined the "porosity thickness" of the chalk as 1.407 cm at the scan position used for this example.

From the 52 kV scan, the photon energy distribution was recorded on 400 MCA channels representing potentials from 29 keV to 52 keV. On a channel-by-channel basis, equation 7 was used to calculate emergent intensity values given I_0 versus potential results from the dry scan and linear absorption coefficient versus potential data of figure 2. The resulting pulse height distributions are shown on figure 3. Note that, although the x-ray generator was set at 52 kV, the 52 keV_p "peak" potential is really the upper bound of the photon distribution plot rather than the potential at which peak intensity occurs. The distribution curves are not symmetric with respect to the peak intensity. For the 95 kV scan, 750 MCA channels representing potentials from 52 keV to 95 keV recorded the photon energy distribution. Again, on a channel-by-channel basis, equation 7 was used to calculate emergent intensity values given I_0 results from the dry scan and linear absorption coefficients from figure 2 data. Figure 3 also shows these results. The spikes on each distribution curve around 60 keV and 70 keV are from primary excitation of elements in the tungsten-target x-ray tube. Note that the intensity distribution curves from the 95 kV set are more symmetric on either side of the peak intensity than those of the 52 kV set, but intensity differences among the fluids are less pronounced.

Figure 4 graphs were constructed by calculating emergent intensities that would result if the chalk core was scanned while saturated with various 8 wt. % CsCl or 8 wt. % KBr brine and decane saturations. The 52 kV_p pulse height distributions for 8% CsCl brine and decane saturations shift in the direction of higher potential as the CsCl brine saturation increases. This is the "beam hardening" effect whereby lower energy photons are quenched as the CsCl brine saturation increases, thereby "hardening" or increasing the mean effective energy of the photon spectrum. This effect diminishes at higher energies as shown by 95 kV results. Comparing figures 4a and 4b, one can see that the CsCl brine is a stronger x-ray absorber than the KBr brine for potentials between 40 and 52 keV. Figure 5 shows pulse height distributions calculated for the same chalk plug for various 8% CsCl brine, decane, and nitrogen gas saturations that would result from scanning the chalk plug with the 52 kV tube potential.

These types of analyses are particularly useful for designing x-ray experiments without having to resort to trial and error fluid injection tests. Using fluids of known compositions, we have found predicted and measured pulse height distributions to be in good agreement.

Integrating Intensities

From the discussions above, it would seem that one could accurately calculate saturations using intensities measured by each MCA channel, as long as the porosity thickness of the rock and absorption coefficients of the fluids are well defined, flux from the x-ray tube is constant, and the detector is perfect. This is certainly possible in theory. Common practice, though, is to integrate or sum intensities over a range of potentials to yield higher intensity values that might be more consistent on an average basis, to simplify data processing and calculations, and to reduce data storage requirements. For example, using an integrated intensity approach, instead of saving and performing calculations on intensity measurements from 400 or more MCA channels for each scan position, intensities are summed from one or more groups of MCA channels and one or more "integrated" intensity values are saved. By taking this approach, however, one assumes that absorption coefficients can be averaged over a range of potentials. Saturation measurement accuracy can be limited by this assumption. To demonstrate this, saturations were calculated from data of figure 4 using an integrated intensity approach. Brine and decane absorption coefficients were calculated from changes in integrated intensity from dry to liquid saturated conditions using equation 7. Next, after using equation 12 to calculate the thickness of brine from each "scan result", brine saturations were computed by dividing each brine thickness by the total fluid filled thickness (1.407 cm in this example). Results are provided in tables 1, 2, and 3. Several interesting results bear discussion. Notice that for conditions of complete brine or complete decane saturation, calculated saturations are in excellent agreement with "true" saturations regardless of ranges of intensity integration. This comes as no surprise since these data sets were used to calculate average linear absorption coefficients for brine and decane initially. However, although the end-point saturations are well matched, saturations can still be in error for data between these end-points. Agreement between true and calculated saturation improves as the integration range is made narrow or for potentials that are within a range on the pulse height distribution curve that is approximately symmetric with respect to peak intensities.

A similar treatment was applied to the three-phase data of figure 5 using two narrow integrated intensity regions. The first region is from 40.03 to 41.02 keV, while the second region is from 49.02 to 50.07 keV. Brine and decane absorption coefficients were calculated for each region from changes in integrated intensity from dry to liquid saturated conditions using equation 7. Saturations were calculated using equations 16, 17, 18 and the approximation of equation 19. Results are presented in table 4. As shown, calculated results are in good agreement with "true" saturations for this example. Typically, however, data noise and variations due to other factors (positioning errors and such) would make high accuracy difficult to achieve using this specific technique for three-phase measurements. Another technique is to use integrated intensities from scans at two different tube potentials, such as 52 kV and 95 kV, to solve for three-phase saturations. By this technique, either the oil phase or brine phase can be doped depending upon test requirements. Another way to improve resolution is to dope oil and

brine phases with different absorbers to increase contrast (differences between linear absorption coefficients) between these fluids at different potentials, such as the methods of Laird and Putnam⁵ and the "dual energy" approach used by Oak and Ehrlich¹⁰. When using any integrated intensity approach, it is useful to record the full emergent spectra for at least one scan position during each core scan to have a means for identifying and correcting for invalid assumptions or changes in absorption coefficients.

Considerations for Reservoir-Condition Tests

For examples shown thus far, reference intensities (I_0) were from dry core scans. It isn't always practical or advantageous to begin a test with a clean, dry core. Because the physics of absorption still applies to native-state corefloods, modifications to the basic approaches of this paper can still be used to calculate saturations during native-state corefloods. When one understands absorption phenomena, a number of options or approaches can be identified for relating fluid saturations to emergent x-ray intensities within core plugs without having to completely saturate cores with brine, oil, or gas.

During reservoir condition tests, particular attention is necessary to accurately calculate saturations from x-ray measurements, especially when test sequences include temperature and pressure changes. For a dead fluid, or one that does not contain solution gas, if the mass absorption coefficient and density of the fluid are known, linear absorption coefficients can be predicted at different pressure and temperature conditions using equation 4 as long as densities are known at these conditions. Likewise, if one knows the mass absorption coefficient of a fluid and can measure linear absorption coefficients at various pressures and temperatures, one can calculate fluid densities for those conditions using equation 4. For tests with live fluids and tests with fluids of unknown composition, a reasonable approach towards quantifying linear absorption coefficients is to scan a known thickness of each fluid and calculate its absorption coefficient directly at test temperature and pressure conditions. For various types of tests, we use a closed-loop system whereby pumps draw fluids from a carbon-fiber/peek/aluminum composite separator for injection into the core sample. Fluids produced from the core return to the separator. The separator is maintained at the same pressure and temperature condition as the coreholder. Scans of the oil-, brine-, and gas-filled portions of the separator provide intensity data for calculating linear absorption coefficients using equation 7.

Any significant changes to the coreholder system also need to be considered in test calculations, including the addition or removal of insulation material and changes in temperature and pressure that affect the absorption characteristics of the confining fluid. A change in the "thickness" or density of the confining fluid within the coreholder will cause a change in emergent x-ray intensity that might be erroneously attributed to a change in saturation conditions within the core. Depending upon the magnitude of the change and the desired accuracy of saturation measurements, it may be necessary to compensate for changes in absorption characteristics of the confining fluid. We have found this to be particularly important during reservoir-condition live fluid

depressurization experiments in which gas evolves within the pore system as a result of pore pressure reduction. To compensate for confining fluid density changes, one can add an additional term in the basic equation for calculations at each energy range,

$$I = I_0 \exp[-\{\sum_i(\mu_i t_i) + \Delta\mu_{\text{confining fluid}} * t_{\text{confining fluid}}\}] \quad (22)$$

or calculate an adjusted baseline intensity (I_0') to adjust for confining fluid density changes.

Conclusions

The following are primary conclusions from this work:

1. Direct application of a form of Lambert's equation provides significant advantages in calculating saturations from x-ray data, compared to heuristic approaches.
2. Methods presented in this paper can be used with polychromatic x-rays.
3. When designing tests in which x-ray data will be recorded using an integrated intensity approach, calculations using the full spectrum of emergent intensities can be used to select ranges of potentials over which integration will be performed to minimize errors introduced because of beam hardening.
4. As linear absorption coefficients are sensitive to density-changing conditions, it is important to consider effects of temperature and pressure changes when designing tests or calculating fluid saturations from x-ray data.
5. The use of absorption coefficients in calculating saturations from x-ray measurements transforms the art of core scanning to a science.

Acknowledgments

The authors express appreciation to the management of Phillips Petroleum Company for supporting the preparation and presentation of this work.

References

1. Boyer, R., F. Morgan, and M. Muskat. "New Method For Measurement of Oil Saturation in Cores." *Trans. AIME* (1947) **170**, p. 15-33.
2. Morgan, F., J. McDowell, and E. Doty. "Improvements in the X-Ray Saturation Technique of Studying Fluid Flow." *Trans. AIME*, (1950), **189**, p. 183-194.
3. Geffen, T. and R. Gladfelter. "X-Ray Absorption Method of Determining Fluid Saturation in Cores." *Trans. AIME*, (1950) **195**, p. 322.
4. Laird, A. and J. Putnam. "Fluid Saturation in Porous Media by X-Ray Technique." *Trans. AIME*, (1951) **192** p. 275-284.
5. Laird, A. and J. Putnam. "Three Component Saturation in Porous Media by X-Ray Techniques." *Trans. AIME*, (1959) **216**, p. 216-220.
6. Maloney, D., D. Wegener, and D. Zornes. "New X-ray Scanning System for Special Core Analyses in Support of Reservoir Characterization." Paper SCA 9940 presented at the 1999 International Symposium of the Society of Core Analysts, Golden, CO (Aug. 1999).
7. Bertin, E. *Principles and Practice of X-ray Spectrometric Analysis*. Plenum Press, New York, (1970).

8. Reiner, I. *Introduction to Matrix Theory and Linear Algebra*. Holt, Rinehart, and Winston, Inc., New York, (1971), p. 32.
9. Berger, M. and J. Hubble. "XCOM: Photon Cross Sections on a Personal Computer." NBSIR 87-3597, (1987). Current XCOM version 3.1 (June, 1999) by M. Berger and M. Seltzer. The program can be downloaded (free) or run from the National Institute of Standards and Technology website at <http://physics.nist.gov/PhysRefData/Xcom/Text/XCOM.html>.
10. Oak, M. and R. Ehrlich. "A New X-Ray Absorption Method for Measurement of Three-Phase Relative Permeability." Paper SPE 14420 presented at the 60th Annual Technical Conference and Exhibition of the Society of Petroleum Engineers, Las Vegas, NV (Sept. 22-25, 1985).

Table 1. Calculated Saturations for 8% CsCl Brine and Decane data of Figure 4a, 52 kV tube potential

| keV Range | 29.01 - 52.21 | 37.71-52.21 | 37.71-51.05 | 45.60-49.95 |
|---|---------------|-------------|-------------|-------------|
| μ_w, cm^{-1} | 1.286 | 1.298 | 1.313 | 1.205 |
| μ_o, cm^{-1} | 0.149 | 0.148 | 0.148 | 0.147 |
| Brine Saturations, S_w (true) versus S_w' (calculated), fraction of pore volume | | | | |
| S_w | S_w' | S_w' | S_w' | S_w' |
| 1.000 | 1.000 | 1.000 | 1.000 | 1.000 |
| 0.800 | 0.807 | 0.804 | 0.804 | 0.801 |
| 0.600 | 0.610 | 0.607 | 0.607 | 0.601 |
| 0.400 | 0.410 | 0.407 | 0.407 | 0.401 |
| 0.200 | 0.207 | 0.205 | 0.205 | 0.201 |
| 0.000 | 0.000 | 0.000 | 0.000 | 0.000 |

Table 2. Calculated Saturations, 8% KBr Brine and Decane data of Figure 4b, 52 kV tube potential

| keV Range | 29.01 - 52.21 | 37.71 - 52.21 | 37.71 - 51.05 | 45.60 - 49.95 |
|---|---------------|---------------|---------------|---------------|
| μ_w, cm^{-1} | 0.550 | 0.535 | 0.540 | 0.495 |
| μ_o, cm^{-1} | 0.149 | 0.148 | 0.148 | 0.147 |
| Brine Saturations, S_w (true) versus S_w' (calculated), fraction of pore volume | | | | |
| S_w | S_w' | S_w' | S_w' | S_w' |
| 1.000 | 1.000 | 1.000 | 1.000 | 1.000 |
| 0.800 | 0.803 | 0.802 | 0.802 | 0.800 |
| 0.600 | 0.605 | 0.603 | 0.602 | 0.600 |
| 0.400 | 0.405 | 0.403 | 0.402 | 0.400 |
| 0.200 | 0.204 | 0.202 | 0.202 | 0.200 |
| 0.000 | 0.000 | 0.000 | 0.000 | 0.000 |

Table 3. Calculated Saturations for 8% CsCl Brine and Decane data of Figure 4a, 95 kV tube potential

| keV Range | 52.21 - 95.71 | 60.91 - 75.41 | 74.43 - 94.38 | 81.81 - 91.42 |
|---|---------------|---------------|---------------|---------------|
| μ_w, cm^{-1} | 0.412 | 0.530 | 0.388 | 0.372 |
| μ_o, cm^{-1} | 0.130 | 0.134 | 0.129 | 0.129 |
| Brine Saturations, S_w (true) versus S_w' (calculated), fraction of pore volume | | | | |
| S_w | S_w' | S_w' | S_w' | S_w' |
| 1.000 | 1.000 | 1.000 | 1.000 | 1.000 |
| 0.800 | 0.802 | 0.801 | 0.801 | 0.800 |
| 0.600 | 0.603 | 0.601 | 0.601 | 0.600 |
| 0.400 | 0.403 | 0.401 | 0.401 | 0.400 |
| 0.200 | 0.202 | 0.201 | 0.201 | 0.200 |
| 0.000 | 0.000 | 0.000 | 0.000 | 0.000 |

Table 4. Calculated Saturations for 8% Brine, Decane, and Nitrogen Gas Data of Figure 5, 52 kV tube potential

| keV Range | 40.03 - 41.02 | | | | | 49.02 - 50.07 | | | | | | | | | | |
|-------------------------|---------------------|-------|--------|-------|-------|---------------------|-------|-------|-------|-------|--------|-------|-------|-------|-------|-------|
| μ_w, cm^{-1} | $\mu_{1,1} = 1.757$ | | | | | $\mu_{2,1} = 1.111$ | | | | | | | | | | |
| μ_o, cm^{-1} | $\mu_{1,2} = 0.154$ | | | | | $\mu_{2,2} = 0.145$ | | | | | | | | | | |
| "True" Saturations | | | | | | | | | | | | | | | | |
| S_w | 1.000 | 0.750 | 0.750 | 0.500 | 0.500 | 0.500 | 0.250 | 0.250 | 0.250 | 0.250 | 0.250 | 0.000 | 0.000 | 0.000 | 0.000 | 0.000 |
| S_o | 0.000 | 0.250 | 0.000 | 0.500 | 0.250 | 0.000 | 0.750 | 0.500 | 0.250 | 0.250 | 0.000 | 1.000 | 0.750 | 0.500 | 0.250 | 0.000 |
| S_g | 0.000 | 0.000 | 0.250 | 0.000 | 0.250 | 0.500 | 0.000 | 0.250 | 0.500 | 0.500 | 0.750 | 0.000 | 0.250 | 0.500 | 0.750 | 1.000 |
| Calculated Saturations | | | | | | | | | | | | | | | | |
| S_w' | 1.000 | 0.750 | 0.750 | 0.500 | 0.500 | 0.500 | 0.250 | 0.250 | 0.250 | 0.250 | 0.250 | 0.000 | 0.000 | 0.000 | 0.000 | 0.000 |
| S_o' | 0.000 | 0.249 | -0.001 | 0.499 | 0.249 | -0.001 | 0.749 | 0.499 | 0.249 | 0.249 | -0.001 | 1.000 | 0.750 | 0.500 | 0.250 | 0.000 |
| S_g' | 0.000 | 0.001 | 0.251 | 0.001 | 0.251 | 0.501 | 0.001 | 0.251 | 0.501 | 0.501 | 0.751 | 0.000 | 0.250 | 0.500 | 0.750 | 1.000 |

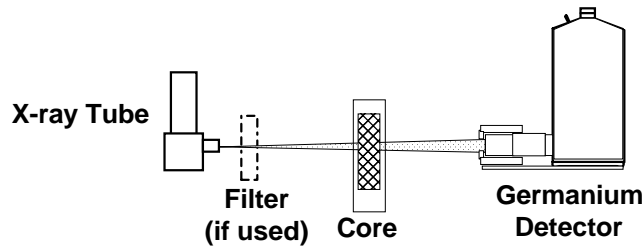


Figure 1. Scan arrangement.

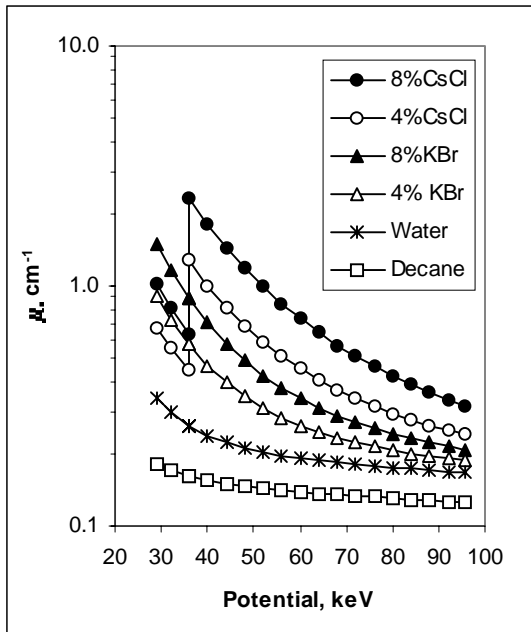


Figure 2. Linear absorption coefficients for various fluids.

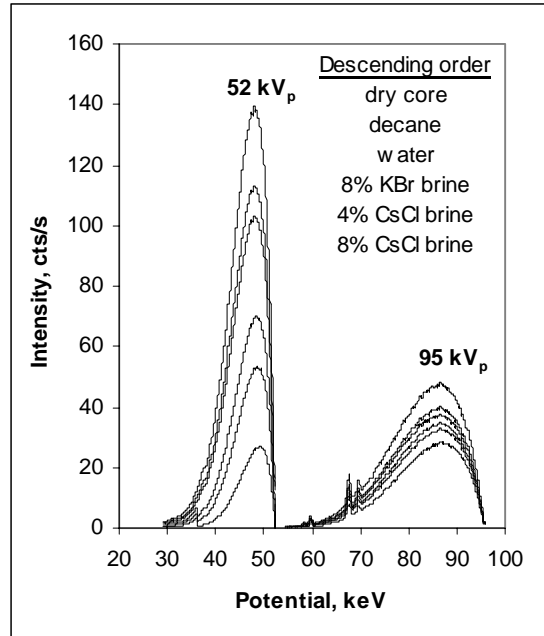
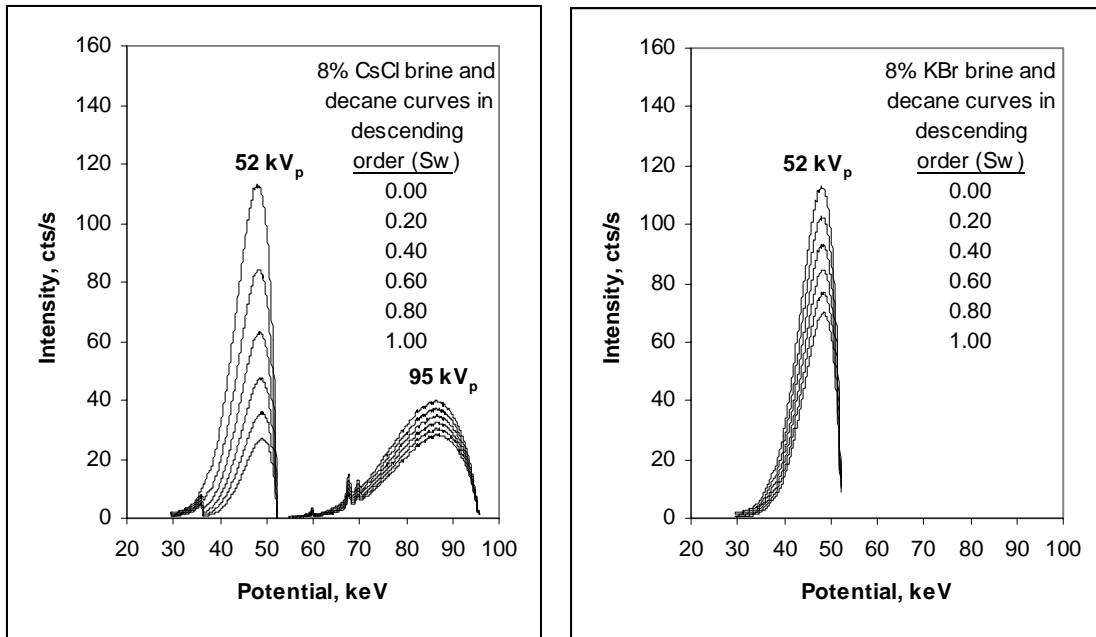


Figure 3. Pulse height distributions for a chalk plug saturated with various fluids.



(a)

(b)

Figure 4. Pulse height distributions for a chalk plug saturated with decane and brine. Side (a) shows 52 kV_p and 95 kV_p results with 8% CsCl brine. Side (b) shows 52 kV_p results with 8% KBr brine.

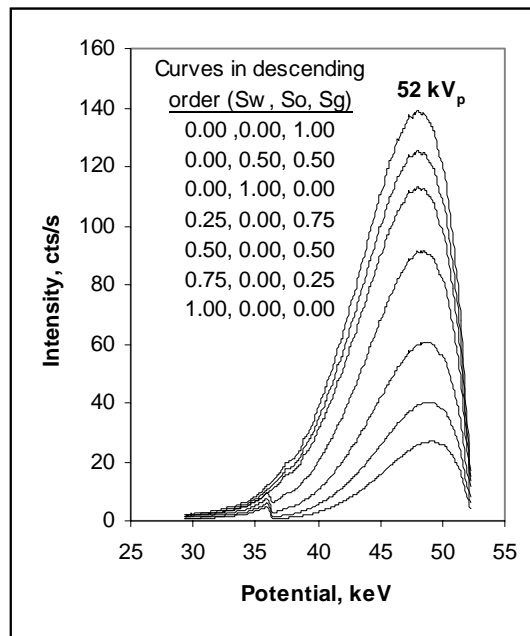


Figure 5. Pulse height curves for various 8% CsCl brine, decane, and N₂ saturations.